Tube-based MPC with Nonlinear Control for Load Transportation using a UAV

Marcelo A. Santos * **Antonio Ferramosca** **
Guilherme V. Raffo *,***

* *Graduate Program in Electrical Engineering, Federal University of Minas Gerais, Belo Horizonte, MG, Brazil (cidomg32@ufmg.br).*
** *CONICET, UTN - Facultad Regional Reconquista, Santa Fe 3560, Argentina (ferramosca@santafe-conicet.gov.ar).*
*** *Department of Electronics Engineering, Federal University of Minas Gerais, Belo Horizonte, MG, Brazil (raffo@ufmg.br).*

Abstract: This paper presents a two-stage cascade control framework to solve hierarchically the trajectory tracking problem of a Tilt-rotor Unmanned Aerial Vehicle (UAV) carrying a suspended load. Initially, a nonlinear dynamic model is presented, which is after decoupled into two subsystems. The outer control system is designed by means of a robust tube-based Model Predictive Control (MPC) strategy, which is used to control the UAV's planar motion and stabilize the suspended load. For the inner control system, the input-output feedback linearization (IOFL) technique combined with the dynamic extension approach and a discrete mixed $\mathcal{H}_2/\mathcal{H}_\infty$ controller is considered to control the UAV's altitude and attitude. Simulations results are carried out to corroborate the proposed control strategy.

Keywords: UAV, Load transportation, Tube-based MPC, Nonlinear Control

1. INTRODUCTION

Unmanned Aerial Vehicles have experienced in recent years a great popularization among academics, hobbyists, and, more recently, in the industries. This is mainly due to the development of technologies related with the design and assembly of these vehicles, for instance, lighter and resistant low-cost materials and more powerful and smaller embedded systems. Consequently, new applications are arising in the civil sphere as: precision agriculture, fire detection, cargo transportation and delivery.

UAVs are found in two main configurations: rotary-wing and fixed-wing. The first has the advantage of performing Vertical Take-Off and Landing (VTOL), while the second one is able to obtain improved forward flights. Some hybrid aircraft have been proposed to combine the VTOL capacity with a larger range, endurance, and forward speed. Amongst them, the Tilt-rotor configuration is one of the most popular, being able of switching between helicopter and airplane flight-modes only by tilting its thrusters group. This kind of aircraft is particularly interesting for load transportation tasks since they present fast deployment and high maneuverability in slow velocities. However, despite their advantages, they also come with control design challenges since these vehicles are complex underactuated mechanical systems with highly coupled and nonlinear dynamics affected by aerodynamic perturbations. Yet,

depending on how the control inputs are selected, control input nonlinearities may appear. Moreover, when a payload is connected to the UAV through a rope, the dynamic behavior of the system varies due to the load's swing and the system's underactuation degree increases.

Only a few works dealing with control design for Tilt-rotor UAVs can be found in the literature (Yanguo and Huanjin, 2009; Amiri et al., 2013; Papachristos et al., 2013). When it comes to the control design of Tilt-rotor UAVs in load transportation tasks, the literature is even more limited. However, if others UAVs structures are considered, works dealing with the load transportation control problem can be found: Dai et al. (2014) and Sreenath et al. (2013) for quadrotors, and Bernard and Kondak (2009) for helicopters.

This paper adapts the two-stage cascade framework proposed in Raffo and Almeida (2018) taking into account in the outer-loop a tube-based MPC strategy, which replaces the initially proposed IOFL with linear $\mathcal{H}_2/\mathcal{H}_\infty$ controller without losing the robustness feature. Moreover, in the inner-loop, a discrete mixed $\mathcal{H}_2/\mathcal{H}_\infty$ controller deals with the linear system obtained through IOFL procedure aiming to avoid additional uncertainties coming from the discretization process. The proposed control strategy must perform trajectory tracking of the Tilt-rotor UAV operating in helicopter flight-mode while keeping the suspended load stable. Besides, it must be robust against modeling uncertainties and constant external disturbances.

2. SYSTEM MODELING

This section briefly describes the equations of motion of a Tilt-rotor UAV with suspended load (further details can

be found in Almeida and Raffo (2015)). The system can be seen as a multi-body mechanical one composed of four bodies (see Fig. 1): the main body, two thrusters' groups, and a suspended load. The system is actuated through the aircraft's thrusters group composed by two servomotors to tilt the propellers and two rotors to generate the lift force. For modeling purposes, all bodies are assumed to be rigid; the load is assumed to be attached to the main body by a massless inelastic rope through two revolute joints; the rope is connected to the aircraft's geometric center; the main body's center of mass does not coincide with the aircraft's geometric center; and the thrusters groups' centers of mass are located at their respective tilting axes.
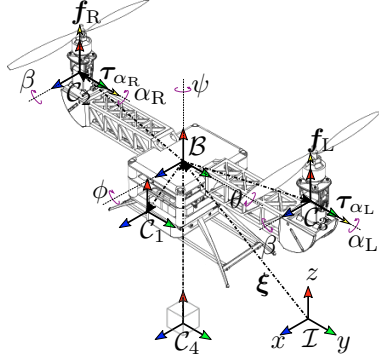
Fig. 1. Tilt-rotor UAV frames and variables definition.

Six frames are defined to describe the system: the inertial frame $\mathcal{I}$, and the moving frames $\mathcal{B}$ and $\mathcal{C}_i$, which are, respectively, frames rigidly attached to the main body center of rotation and to the center of mass of the i-th body (see Fig. 1). The position of the body frame's origin represented in $\mathcal{I}$ is given by $\boldsymbol{\xi} = [x\ y\ z]'$ and the attitude by $\boldsymbol{\eta} = [\phi\ \theta\ \psi]'$. The orientation of $\mathcal{C}_2$ and $\mathcal{C}_3$ w.r.t. $\mathcal{B}$ are obtained by rotations α_R and α_L around $Y^{\mathcal{B}}$-axis, and constant tilts $-\beta$ and β around the $X^{\mathcal{B}}$-axis, respectively. Moreover, considering the load as a pendulum with length l and two degrees of freedom represented by γ_1 and γ_2 (rotations around $X^{\mathcal{B}}$-axis and $Y^{\mathcal{B}}$-axis, respectively), the position of the suspended load w.r.t $\mathcal{B}$ becomes a simple forward kinematic problem.

Thus, the generalized coordinates describing the Tilt-rotor UAV motion are chosen as $\boldsymbol{q} = [\boldsymbol{\xi}'\ \boldsymbol{\eta}'\ \alpha_R\ \alpha_L\ \gamma_1\ \gamma_2]'$. Moreover, the system's inputs are $\boldsymbol{u} = [f_R\ f_L\ \tau_R\ \tau_L]'$, with f_R and f_L being the thrust forces and τ_R and τ_L the torques.

The dynamic model of the Tilt-rotor UAV with suspended load can be described by the Euler-Lagrange equation as

$$\boldsymbol{M}(\boldsymbol{q})\,\ddot{\boldsymbol{q}} + \boldsymbol{C}(\boldsymbol{q},\dot{\boldsymbol{q}})\,\dot{\boldsymbol{q}} + \boldsymbol{G}(\boldsymbol{q}) = \boldsymbol{\vartheta}(\boldsymbol{q},\dot{\boldsymbol{q}}), \tag{1}$$

where $\boldsymbol{M}(\boldsymbol{q})$ is the inertia matrix, $\boldsymbol{C}(\boldsymbol{q},\dot{\boldsymbol{q}})$ is the Coriolis and centripetal forces matrix, $\boldsymbol{G}(\boldsymbol{q})$ is the gravitational force vector, and $\boldsymbol{\vartheta}(\boldsymbol{q},\dot{\boldsymbol{q}})$ is the forces and torques vector.

The inertia matrix $\boldsymbol{M}(\boldsymbol{q})$ can be written as

$$\boldsymbol{M}(\boldsymbol{q}) = \begin{bmatrix} m\boldsymbol{I}_{3\times3} & \boldsymbol{m}_{12} & \boldsymbol{0}_{3\times1} & \boldsymbol{0}_{3\times1} & m_4\boldsymbol{R}_{\mathcal{B}}^{\mathcal{I}}\boldsymbol{L} \\ * & \boldsymbol{W}_\eta'\boldsymbol{J}\boldsymbol{W}_\eta & \boldsymbol{m}_{23} & \boldsymbol{m}_{24} & \boldsymbol{m}_{25} \\ * & * & \vec{\boldsymbol{j}}'\boldsymbol{I}_2\vec{\boldsymbol{j}} & 0 & \boldsymbol{0}_{1\times2} \\ * & * & * & \vec{\boldsymbol{j}}'\boldsymbol{I}_3\vec{\boldsymbol{j}} & \boldsymbol{0}_{1\times2} \\ * & * & * & * & \boldsymbol{m}_{55} \end{bmatrix}, \tag{2}$$

where the $*$ terms indicate symmetry w.r.t. the main diagonal, $\boldsymbol{m}_{12} = -\boldsymbol{R}_{\mathcal{B}}^{\mathcal{I}}\boldsymbol{H}\boldsymbol{W}_\eta$, $\boldsymbol{m}_{23} = \boldsymbol{W}_\eta'\boldsymbol{R}_{\mathcal{C}_2}^{\mathcal{B}}\boldsymbol{I}_2\vec{\boldsymbol{j}}$, $\boldsymbol{m}_{24} =$

$\boldsymbol{W}_\eta'\boldsymbol{R}_{\mathcal{C}_3}^{\mathcal{B}}\boldsymbol{I}_3\vec{\boldsymbol{j}}$, $\boldsymbol{m}_{25} = \boldsymbol{W}_\eta'\boldsymbol{R}_{\mathcal{C}_4}^{\mathcal{B}}\boldsymbol{I}_4\boldsymbol{P} + m_4\boldsymbol{W}_\eta'\boldsymbol{S}(\boldsymbol{d}_{\mathcal{C}_4}^{\mathcal{B}})\boldsymbol{L}$, $\boldsymbol{m}_{55} = m_4\boldsymbol{L}'\boldsymbol{L} + \boldsymbol{P}'\boldsymbol{I}_4\boldsymbol{P}$. Moreover, $\boldsymbol{S}(\cdot)$ denotes a skew symmetric matrix; $\boldsymbol{R}_j^i$ denotes the rotation matrix between the frames j and i; $\boldsymbol{d}_j^i$ denotes the distance between the frames i and j expressed in i; $\vec{\boldsymbol{i}}$, $\vec{\boldsymbol{j}}$, and $\vec{\boldsymbol{k}}$ denote, respectively, unit vectors along X, Y, and Z axes; $m = \sum m_i$; $\boldsymbol{J} = \sum \boldsymbol{J}_i$ and $\boldsymbol{H} = \boldsymbol{S}(\sum m_i\boldsymbol{d}_{\mathcal{C}_i}^{\mathcal{B}})$, with $\boldsymbol{J}_i = \boldsymbol{R}_{\mathcal{C}_i}^{\mathcal{B}}\boldsymbol{I}_i(\boldsymbol{R}_{\mathcal{C}_i}^{\mathcal{B}})' + m_i\boldsymbol{S}(\boldsymbol{d}_{\mathcal{C}_i}^{\mathcal{B}})'\boldsymbol{S}(\boldsymbol{d}_{\mathcal{C}_i}^{\mathcal{B}})$ being the inertia tensor of the i-th body with moment of inertia $\boldsymbol{I}_i$ and mass m_i; and

$$\boldsymbol{W}_\eta = \begin{bmatrix} 1 & 0 & -s_\theta \\ 0 & c_\phi & s_\phi c_\theta \\ 0 & -s_\phi & c_\phi c_\theta \end{bmatrix},\ \boldsymbol{P} = \begin{bmatrix} 1 & 0 \\ 0 & c_{\gamma_1} \\ 0 & -s_{\gamma_1} \end{bmatrix},\ \boldsymbol{L} = \begin{bmatrix} ls_{\gamma_1}s_{\gamma_2} & -lc_{\gamma_1}c_{\gamma_2} \\ lc_{\gamma_1} & 0 \\ ls_{\gamma_1}c_{\gamma_2} & lc_{\gamma_1}s_{\gamma_2} \end{bmatrix}.$$

Moreover, the matrix $\boldsymbol{C}(\boldsymbol{q},\dot{\boldsymbol{q}})$ can be obtained directly from (2) using the Christoffel symbols of the first kind, while the gravitational vector can be obtained from the system's potential energy $\mathcal{U}$ as $\boldsymbol{G}(\boldsymbol{q}) = \partial\mathcal{U}/\partial\boldsymbol{q}$, with $\mathcal{U} = (\boldsymbol{g}^{\mathcal{I}})'\boldsymbol{R}_{\mathcal{B}}^{\mathcal{I}}(\sum_{i=1}^{4}m_i\boldsymbol{d}_{\mathcal{C}_i}^{\mathcal{B}}) + (\boldsymbol{g}^{\mathcal{I}})'m\boldsymbol{\xi}$, where $\boldsymbol{g} = [0\ 0\ -g_z]'$ denotes the gravitational acceleration.

Furthermore, the generalized forces and torques vector $\boldsymbol{\vartheta}(\boldsymbol{q},\dot{\boldsymbol{q}})$ can be described as a combination of forces and torques generated by the actuators, $\boldsymbol{\vartheta}_{\boldsymbol{u}}$, the friction between the rope and the Tilt-rotor, $\boldsymbol{\vartheta}_{\boldsymbol{fr}}$, and the external disturbances applied to the vehicle, $\boldsymbol{\vartheta}_{\boldsymbol{d}}$. Hence, the generalized forces and torques vector can be expressed as

$$\boldsymbol{\vartheta} = \boldsymbol{\vartheta}_{\boldsymbol{u}} + \boldsymbol{\vartheta}_{\text{fr}} + \boldsymbol{\vartheta}_{\text{d}}, \tag{3}$$

where

$$\boldsymbol{\vartheta}_{\boldsymbol{u}} = \boldsymbol{B}\boldsymbol{u} = \begin{bmatrix} \boldsymbol{R}_{\mathcal{B}}^{\mathcal{I}}\boldsymbol{r}_R & \boldsymbol{R}_{\mathcal{B}}^{\mathcal{I}}\boldsymbol{r}_L & \boldsymbol{0}_{2\times2} \\ \boldsymbol{W}_\eta'\boldsymbol{\tau}_R & \boldsymbol{W}_\eta'\boldsymbol{\tau}_L & \\ \hline \boldsymbol{0}_{2\times2} & \boldsymbol{I}_{2\times2} \\ \boldsymbol{0}_{2\times2} & \boldsymbol{0}_{2\times2} \end{bmatrix} \begin{bmatrix} f_R \\ f_L \\ \tau_{\alpha_R} \\ \tau_{\alpha_L} \end{bmatrix}, \tag{4}$$

$$\boldsymbol{\vartheta}_{\text{fr}} = -\boldsymbol{\mu}\dot{\boldsymbol{q}} = -\mathbf{blkdiag}(0,0,0,0,0,0,0,0,\mu_\gamma,\mu_\gamma)\dot{\boldsymbol{q}}, \tag{5}$$

$$\boldsymbol{\vartheta}_{\text{d}} = [\boldsymbol{I}_{3\times3}\ \boldsymbol{0}_{3\times3}\ \boldsymbol{0}_{3\times2}\ \boldsymbol{0}_{3\times2}]'\boldsymbol{d}, \tag{6}$$

with $\boldsymbol{d} = [d_x\ d_y\ d_z]'$ denoting the disturbance vector, and

$$\boldsymbol{r}_R = [s_{\alpha_R}\ c_{\alpha_R}s_\beta\ c_{\alpha_R}c_\beta]',\ \boldsymbol{r}_L = [s_{\alpha_L}\ -c_{\alpha_L}s_\beta\ c_{\alpha_L}c_\beta]',$$

$$\boldsymbol{\tau}_R = \begin{bmatrix} -c_{\alpha_R}c_\beta d^y - k_d s_{\alpha_R} \\ s_{\alpha_R}d^z + k_d c_{\alpha_R}s_\beta \\ s_{\alpha_R}d^y + k_d c_{\alpha_R}c_\beta \end{bmatrix},\ \boldsymbol{\tau}_L = \begin{bmatrix} c_{\alpha_L}c_\beta d^y + k_d s_{\alpha_L} \\ s_{\alpha_L}d^z - k_d c_{\alpha_L}s_\beta \\ -s_{\alpha_L}d^y - k_d c_{\alpha_L}c_\beta \end{bmatrix},$$

being $d^z = d_{\mathcal{C}_2,z}^{\mathcal{B}} = d_{\mathcal{C}_3,z}^{\mathcal{B}}$, $d^y = |d_{\mathcal{C}_2,y}^{\mathcal{B}}|$, with $\boldsymbol{d}_{j,k}^i$ denoting the $k \in \{x,y,z\}$ component of the distance vector $\boldsymbol{d}_j^i$, and k_d an aerodynamic constant.

3. CASCADE STRUCTURE

This section briefly presents the two-level cascade control framework proposed by Raffo and Almeida (2018). The outer-loop is designed in order to control x and y while stabilizing the angles γ_1 and γ_2 actuating on the desired roll and pitch angles to be set as a reference for the inner-loop. Besides, the inner-loop controls $\boldsymbol{\eta}$ and z while stabilizing the angles α_R and α_L actuating on the inputs $\boldsymbol{u}$.

Aiming to decouple the system (1) into two independent subsystems, it is assumed that (Raffo and Almeida, 2018):

A1. The coupling between the attitude and position dynamics is negligible ($\boldsymbol{m}_{12} = \boldsymbol{R}_{\mathcal{B}}^{\mathcal{I}}\boldsymbol{H}\boldsymbol{W}_\eta \approx \boldsymbol{0}$).

A2. The coupling between the altitude and load angles dynamics is negligible ($\boldsymbol{m}_{15} \approx [\vec{\boldsymbol{i}}\ \vec{\boldsymbol{j}}\ \boldsymbol{0}]\boldsymbol{m}_{15}$).

A3. The coupling between the attitude and tilting angles dynamics is negligible ($\boldsymbol{m}_{23} \approx \boldsymbol{0}$ and $\boldsymbol{m}_{24} \approx \boldsymbol{0}$).

A4. The coupling between the attitude and the load motion dynamics is negligible ($\boldsymbol{m}_{25} \approx \boldsymbol{0}$).

Thereafter, Eq. (1) can be split into two new decoupled models with the generalized coordinates $\boldsymbol{q}_1 = \begin{bmatrix} z & \boldsymbol{\eta}' & \alpha_R & \alpha_L \end{bmatrix}'$ and $\boldsymbol{q}_2 = \begin{bmatrix} x & y & \gamma_1 & \gamma_2 \end{bmatrix}'$, yielding to

$$\boldsymbol{M}_{\boldsymbol{q}_1}(\boldsymbol{q}_1)\,\ddot{\boldsymbol{q}}_1 + \boldsymbol{C}_{\boldsymbol{q}_1}(\boldsymbol{q}_1,\dot{\boldsymbol{q}}_1)\,\dot{\boldsymbol{q}}_1 + \boldsymbol{G}_{\boldsymbol{q}_1}(\boldsymbol{q}_1) = \boldsymbol{\vartheta}_{\boldsymbol{q}_1}(\boldsymbol{q}_1,\dot{\boldsymbol{q}}_1), \quad (7)$$

$$\boldsymbol{M}_{\boldsymbol{q}_2}(\boldsymbol{q}_2)\,\ddot{\boldsymbol{q}}_2 + \boldsymbol{C}_{\boldsymbol{q}_2}(\boldsymbol{q}_2,\dot{\boldsymbol{q}}_2)\,\dot{\boldsymbol{q}}_2 + \boldsymbol{G}_{\boldsymbol{q}_2}(\boldsymbol{q}_2) = \boldsymbol{\vartheta}_{\boldsymbol{q}_2}(\boldsymbol{q}_2,\dot{\boldsymbol{q}}_2), \quad (8)$$

where $\boldsymbol{M}_{\boldsymbol{q}_i} = \boldsymbol{I}_{\boldsymbol{q}_i}\boldsymbol{M}\boldsymbol{I}'_{\boldsymbol{q}_i}$, $\boldsymbol{C}_{\boldsymbol{q}_i} = \boldsymbol{I}_{\boldsymbol{q}_i}\boldsymbol{C}\boldsymbol{I}'_{\boldsymbol{q}_i}$, $\boldsymbol{G}_{\boldsymbol{q}_i} = \boldsymbol{I}_{\boldsymbol{q}_i}\boldsymbol{G}$, and $\boldsymbol{\vartheta}_{\boldsymbol{q}_i} = \boldsymbol{I}_{\boldsymbol{q}_i}\boldsymbol{\vartheta}$ with

$$\boldsymbol{I}_{\boldsymbol{q}_1} = \begin{bmatrix} \boldsymbol{0}_{6\times 2} & \boldsymbol{I}_{6\times 6} & \boldsymbol{0}_{6\times 2} \end{bmatrix} \quad \text{and} \quad \boldsymbol{I}_{\boldsymbol{q}_2} = \begin{bmatrix} \boldsymbol{I}_{2\times 2} & \boldsymbol{0}_{2\times 6} & \boldsymbol{0}_{2\times 2} \\ \boldsymbol{0}_{2\times 2} & \boldsymbol{0}_{2\times 6} & \boldsymbol{I}_{2\times 2} \end{bmatrix}.$$

Considering (3) with (4) - (6), $\boldsymbol{\vartheta}_{\boldsymbol{q}_i}$ can be expressed as

$$\boldsymbol{\vartheta}_{\boldsymbol{q}_i} = \boldsymbol{B}_{\boldsymbol{q}_i}\boldsymbol{u} - \boldsymbol{\mu}_{\boldsymbol{q}_i}\dot{\boldsymbol{q}}_i + \boldsymbol{\delta}_{\boldsymbol{q}_i}, \quad (9)$$

where $\boldsymbol{B}_{\boldsymbol{q}_i} = \boldsymbol{I}_{\boldsymbol{q}_i}\boldsymbol{B}$, $\boldsymbol{\mu}_{\boldsymbol{q}_i} = \boldsymbol{I}_{\boldsymbol{q}_i}\boldsymbol{\mu}\boldsymbol{I}'_{\boldsymbol{q}_i}$, and $\boldsymbol{\delta}_{\boldsymbol{q}_i}$ is a vector containing the unmodeled dynamics from the decoupled procedure and the external disturbances $\boldsymbol{\vartheta}_{\mathrm{d}}$.

Using (9), the decoupled models (7) and (8) can be rewritten in the state-space form as [1]

$$\dot{\boldsymbol{x}}_{\boldsymbol{q}_i} = \begin{bmatrix} \dot{\boldsymbol{q}}_i \\ \ddot{\boldsymbol{q}}_i \end{bmatrix} = \begin{bmatrix} \dot{\boldsymbol{q}}_i \\ \boldsymbol{M}_{\boldsymbol{q}_i}^{-1}\left[\boldsymbol{B}_{\boldsymbol{q}_i}\boldsymbol{u} + \boldsymbol{\delta}_{\boldsymbol{q}_i} - [\boldsymbol{C}_{\boldsymbol{q}_i} + \boldsymbol{\mu}_{\boldsymbol{q}_i}]\dot{\boldsymbol{q}}_i - \boldsymbol{G}_{\boldsymbol{q}_i}\right] \end{bmatrix}$$
$$= \boldsymbol{f}_{\boldsymbol{q}_i}(\boldsymbol{x}_{\boldsymbol{q}_i}) + \boldsymbol{g}_{\boldsymbol{u}_{\boldsymbol{q}_i}}\boldsymbol{u} + \boldsymbol{g}_{\boldsymbol{d}_{\boldsymbol{q}_i}}\boldsymbol{\delta}_{\boldsymbol{q}_i}. \quad (10)$$

4. TUBE-BASED MPC OUTER-LOOP CONTROLLER

This section deals with the design of a robust MPC strategy to control the outer-loop dynamics (8). The tube-based approach is used to obtain an MPC strategy robust against additive uncertainties from the unmodeled dynamics, decoupling, linearization, and discretization procedures. When compared to some others robustified MPC approaches, the tube-based one is less conservative and more computationally efficient (Langson et al., 2004).

The tube-based MPC considers the states' trajectory of the nominal and the uncertain systems as different, and the mismatch between them needs to be controlled. Therefore, the control law applied to the system is composed of a pre-stabilizing control policy dealing with the nominal system and an additional control policy compensating the mismatch error (Gonzalez et al., 2011).

4.1 Input affine representation

The outer-loop model (8) is not affine in the inputs ϕ and θ, which prevents to design a controller to regulate the planar movements while stabilizing the load. However, from (4), the effect of the generalized forces on (8) can be written as $\boldsymbol{I}_{\boldsymbol{q}_2}\boldsymbol{B}\boldsymbol{u} = \begin{bmatrix} \boldsymbol{T}_x^{\mathcal{I}} & \boldsymbol{T}_y^{\mathcal{I}} & 0 & 0 \end{bmatrix}'$, with $\boldsymbol{T}_x^{\mathcal{I}}$ and $\boldsymbol{T}_y^{\mathcal{I}}$ being, respectively, translational forces along $\mathrm{X}^{\mathcal{B}}$ and $\mathrm{Y}^{\mathcal{B}}$ axes expressed in $\mathcal{I}$. Additionally, these translational forces can be written as

$$\begin{bmatrix} \boldsymbol{T}_x^{\mathcal{I}} \\ \boldsymbol{T}_y^{\mathcal{I}} \end{bmatrix} = \begin{bmatrix} r_{11} & r_{12} & r_{13} \\ r_{21} & r_{22} & r_{23} \end{bmatrix}(\boldsymbol{r}_R f_R + \boldsymbol{r}_L f_L),$$

where r_{ij} is the (i,j)-th entry of the matrix $\boldsymbol{R}_{\mathcal{B}}^{\mathcal{I}}$. Therefore, decomposing the generalized forces into the projections $f_x^{\mathcal{B}}$, $f_y^{\mathcal{B}}$, and $f_z^{\mathcal{B}}$, it is possible to control the planar movements

and stabilize the load by actuating on the angles ϕ and θ in order to change the projection of $f_z^{\mathcal{B}}$ along the $\mathrm{X}^{\mathcal{I}}$ and $\mathrm{Y}^{\mathcal{I}}$ axes. The remaining projections are assumed to be known disturbances compensated by the controller.

Considering (9), Eq. (8) can be rewritten as

$$\boldsymbol{M}\ddot{\boldsymbol{q}} + [\boldsymbol{C} + \boldsymbol{\mu}]\dot{\boldsymbol{q}} + \boldsymbol{G} - \boldsymbol{F}_{xy} = \boldsymbol{F}_z + \boldsymbol{\delta},$$

where $\boldsymbol{F}_{xy} = \begin{bmatrix} r_{11}f_x^{\mathcal{B}} + r_{12}f_y^{\mathcal{B}} & r_{21}f_x^{\mathcal{B}} + r_{22}f_y^{\mathcal{B}} & 0 & 0 \end{bmatrix}'$ and $\boldsymbol{F}_z = \begin{bmatrix} r_{13}f_z^{\mathcal{B}} & r_{23}f_z^{\mathcal{B}} & 0 & 0 \end{bmatrix}'$. Moreover, defining the auxiliary vector $\boldsymbol{n} = \begin{bmatrix} n_x & n_y & n_{\gamma_1} & n_{\gamma_2} \end{bmatrix}' = [\boldsymbol{C} + \boldsymbol{\mu}]\dot{\boldsymbol{q}} + \boldsymbol{G} - \boldsymbol{F}_{xy}$, the outer-loop model can be rewritten as

$$\boldsymbol{M}\ddot{\boldsymbol{q}} + \boldsymbol{n} = \boldsymbol{F}_z + \boldsymbol{\delta}. \quad (11)$$

Since the nonlinear model (11) cannot be easily expressed as affine in control inputs ϕ and θ, the intermediary input variables Υ_1 and Υ_2 are defined as

$$\begin{aligned} \Upsilon_1 &= \left(s_\psi s_\phi + c_\psi s_\theta c_\phi\right) f_z^{\mathcal{B}} - n_x, \\ \Upsilon_2 &= \left(s_\psi s_\theta c_\phi - c_\psi s_\phi\right) f_z^{\mathcal{B}} - n_y, \end{aligned} \quad (12)$$

forming an algebraic system which solution is given by

$$\begin{aligned} \phi &= \arcsin\left[\sigma\left(\frac{s_\psi(\Upsilon_1+n_x) - c_\psi(\Upsilon_2+n_y)}{f_z^{\mathcal{B}}}\right)\right], \\ \theta &= \arcsin\left[\sigma\left(\frac{c_\psi(\Upsilon_1+n_x) + s_\psi(\Upsilon_2+n_y)}{f_z^{\mathcal{B}} c_\phi}\right)\right], \end{aligned} \quad (13)$$

where $\sigma(a) = \min(1, \max(-1, a))$ is a saturation function.

To evaluate (13), the projections $f_i^{\mathcal{B}}$ with $i \in \{x, y, z\}$ are assumed to be known, allowing to simply obtain the terms n_x and n_y. Moreover, ψ is assumed to be measurable.

Replacing (12) in (11), the outer-loop model becomes

$$\boldsymbol{M}\ddot{\boldsymbol{q}} + \bar{\boldsymbol{n}} = \boldsymbol{\Upsilon} + \boldsymbol{\delta}, \quad (14)$$

where $\bar{\boldsymbol{n}}_{\boldsymbol{q}_2} = \begin{bmatrix} 0 & 0 & n_{\gamma_1} & n_{\gamma_2} \end{bmatrix}'$ and $\boldsymbol{\Upsilon} = \begin{bmatrix} \Upsilon_1 & \Upsilon_2 & 0 & 0 \end{bmatrix}'$.

4.2 Discrete linearized model

In order to implement the tube-based MPC, the model (14) must be rewritten in a state-space representation and its equilibrium point must be found. Therefore,

$$\dot{\boldsymbol{x}} = \boldsymbol{\varphi}(\boldsymbol{x}, \boldsymbol{\Upsilon}, \boldsymbol{\delta}) = \begin{bmatrix} \dot{\boldsymbol{q}} \\ \ddot{\boldsymbol{q}} \end{bmatrix} = \begin{bmatrix} \dot{\boldsymbol{q}} \\ \boldsymbol{M}^{-1}[\boldsymbol{\Upsilon} + \boldsymbol{\delta} - \bar{\boldsymbol{n}}] \end{bmatrix}. \quad (15)$$

Considering the vehicle in hover-flight ($\dot{\boldsymbol{x}} = \boldsymbol{0}$) and not affected by any external disturbances ($\boldsymbol{\delta} = \boldsymbol{0}$), the equilibrium point can be obtained by solving the algebraic problem $\boldsymbol{\varphi}(\boldsymbol{x}, \boldsymbol{\Upsilon}, \boldsymbol{\delta}) = \boldsymbol{0}$, whose solution is given by an infinity set of real numbers since it has more unknown variables than equations. Thus, letting x and y assume any value, the equilibrium values are $\gamma_1^{eq} = 0.000154$, $\gamma_2^{eq} = 0.0411$, $\Upsilon_1^{eq} = \Upsilon_2^{eq} = 0$.

Thereafter, the system (15) can be linearized around a reference trajectory, yielding to

$$\Delta\dot{\boldsymbol{x}} = \boldsymbol{A}(\boldsymbol{\zeta}(t))\Delta\boldsymbol{x} + \boldsymbol{B}(\boldsymbol{\zeta}(t))\Delta\boldsymbol{\Upsilon},$$

where $\Delta\boldsymbol{x} = \boldsymbol{x} - \boldsymbol{x}^{tr}$, $\Delta\boldsymbol{\Upsilon} = \boldsymbol{\Upsilon} - \boldsymbol{\Upsilon}^{tr}$, with $\boldsymbol{x}^{tr} = [(\boldsymbol{q}^{tr})' \ (\dot{\boldsymbol{q}}^{tr})']'$ and $\boldsymbol{\Upsilon}^{tr} = \boldsymbol{M}\ddot{\boldsymbol{q}}^{tr} + \bar{\boldsymbol{n}}$, being $\boldsymbol{q}^{tr}$, $\dot{\boldsymbol{q}}^{tr}$, and $\ddot{\boldsymbol{q}}^{tr}$ provided reference signals with $\boldsymbol{q}^{tr} = [x^{tr}(t) \ y^{tr}(t) \ \gamma_1^{eq} \ \gamma_2^{eq}]'$. For the considered reference trajectory, $\boldsymbol{\zeta}(t)$ is a time-varying vector limited by the polytope $\Delta \in \mathbb{R}^2$ and given by $\boldsymbol{\zeta}(t) = [\ddot{x}^{tr}(t) \ \ddot{y}^{tr}(t)]'$. Further, the linearized Jacobians are given by

$$\boldsymbol{A}(\boldsymbol{\zeta}(t)) = \left.\frac{\partial\boldsymbol{\varphi}(\boldsymbol{x},\boldsymbol{\Upsilon},\boldsymbol{\delta})}{\partial\boldsymbol{x}}\right|_{\substack{\boldsymbol{x}=\boldsymbol{x}^{tr}\\\boldsymbol{\Upsilon}=\boldsymbol{\Upsilon}^{tr}}}, \quad \boldsymbol{B}(\boldsymbol{\zeta}(t)) = \left.\frac{\partial\boldsymbol{\varphi}(\boldsymbol{x},\boldsymbol{\Upsilon},\boldsymbol{\delta})}{\partial\boldsymbol{\Upsilon}}\right|_{\substack{\boldsymbol{x}=\boldsymbol{x}^{tr}\\\boldsymbol{\Upsilon}=\boldsymbol{\Upsilon}^{tr}}},$$

which can be rewritten in a convex polytopic form as $\boldsymbol{A}(\boldsymbol{\zeta}(t)) = \sum_{i=1}^4 \iota_i\boldsymbol{A}_i$, $\boldsymbol{B}(\boldsymbol{\zeta}(t)) = \sum_{i=1}^4 \iota_i\boldsymbol{B}_i$, with $\boldsymbol{A}_i$ and $\boldsymbol{B}_i$ being, respectively, the matrices $\boldsymbol{A}(\boldsymbol{\zeta}(t))$ and $\boldsymbol{B}(\boldsymbol{\zeta}(t))$

---

[1] In the following sections, the subscripts $\boldsymbol{q}_1$ and $\boldsymbol{q}_2$ will be dropped in order to simplify the notation. However, the subsystems can be easily differed by context.

evaluated at the i-th vertex of Δ. Moreover, the constraints $0 \leq \iota_i \leq 1$ and $\sum_{i=1}^{4} \iota_i = 1$ must hold for all i.

Aiming to improve the trajectory tracking performance, the state vector is augmented with integral actions $\Delta \hat{\boldsymbol{x}} = \begin{bmatrix} \Delta \boldsymbol{x}' & \int \left(x - x^{tr} \right) & \int \left(y - y^{tr} \right) \end{bmatrix}'$, whose dynamics are given by

$$\Delta \dot{\hat{\boldsymbol{x}}} = \underbrace{\begin{bmatrix} \boldsymbol{A}(\boldsymbol{\zeta}(t)) & \boldsymbol{0}_{8\times 2} \\ \begin{matrix} 1 & 0 \\ 0 & 1 \end{matrix} & \boldsymbol{0}_{2\times 6} & \boldsymbol{0}_{2\times 2} \end{bmatrix}}_{\hat{\boldsymbol{A}}(\boldsymbol{\zeta}(t))} \Delta \hat{\boldsymbol{x}} + \underbrace{\begin{bmatrix} \boldsymbol{B}(\boldsymbol{\zeta}(t)) \\ \boldsymbol{0}_{2\times 2} \end{bmatrix}}_{\hat{\boldsymbol{B}}(\boldsymbol{\zeta}(t))} \Delta \boldsymbol{\Upsilon}. \quad (16)$$

Finally, the discrete outer-loop linearized model can be obtained after mapping (16) from the continuous-time to the discrete-time domain, yielding to

$$\Delta \hat{\boldsymbol{x}}_{k+1} = \hat{\boldsymbol{A}}(\boldsymbol{\zeta}_k)\Delta \hat{\boldsymbol{x}}_k + \hat{\boldsymbol{B}}(\boldsymbol{\zeta}_k)\Delta \boldsymbol{\Upsilon}_k, \quad (17)$$

being $\hat{\boldsymbol{A}}(\boldsymbol{\zeta}_k)$ and $\hat{\boldsymbol{B}}(\boldsymbol{\zeta}_k)$ obtained after discretizing the model using the Euler approximation with sampling time T_{so}.

4.3 Mismatch error model

Consider the model (17) with additive uncertainties

$$\Delta \hat{\boldsymbol{x}}_{k+1} = \hat{\boldsymbol{A}}(\boldsymbol{\zeta}_k)\Delta \hat{\boldsymbol{x}}_k + \hat{\boldsymbol{B}}(\boldsymbol{\zeta}_k)\Delta \boldsymbol{\Upsilon}_k + \boldsymbol{w}_k, \quad (18)$$

where $\Delta \hat{\boldsymbol{x}} \in \mathbb{E} \subset \mathbb{R}^{10}$, $\Delta \boldsymbol{\Upsilon} \in \mathbb{V} \subset \mathbb{R}^2$, and $\boldsymbol{w} \in \mathbb{W} \subset \mathbb{R}^{10}$, with $\mathbb{E}$, $\mathbb{V}$, and $\mathbb{W}$ being compact sets. The nominal linear error model is obtained from (18) disregarding additive uncertainties

$$\Delta \hat{\boldsymbol{x}}_{k+1}^{nom} = \hat{\boldsymbol{A}}(\boldsymbol{\zeta}_k)\Delta \hat{\boldsymbol{x}}_k^{nom} + \hat{\boldsymbol{B}}(\boldsymbol{\zeta}_k)\boldsymbol{g}_k, \quad (19)$$

where $\Delta \hat{\boldsymbol{x}}_k^{nom} = \hat{\boldsymbol{x}}_k^{nom} - \hat{\boldsymbol{x}}_k^{tr}$ with the superscript $(\cdot)^{nom}$ denoting the nominal state vector, and $\boldsymbol{g}_k$ is the policy able to control the nominal system.

The mismatch error between the uncertain system (18) and the nominal system (19) can be defined as

$$\begin{aligned} \hat{\boldsymbol{e}}_{k+1} &= \Delta \hat{\boldsymbol{x}}_{k+1} - \Delta \hat{\boldsymbol{x}}_{k+1}^{nom} \\ &= \hat{\boldsymbol{A}}(\boldsymbol{\zeta}_k)\hat{\boldsymbol{e}}_k + \hat{\boldsymbol{B}}(\boldsymbol{\zeta}_k)\left[\Delta \boldsymbol{\Upsilon}_k - \boldsymbol{g}_k\right] + \boldsymbol{w}_k. \end{aligned}$$

Since the control objective is to compensate the mismatch error $\hat{\boldsymbol{e}}_k$ while controlling the nominal system through some desired trajectory, the control input for the uncertain system can be defined as (Gonzalez et al., 2011)

$$\Delta \boldsymbol{\Upsilon}_k = \boldsymbol{K}(\boldsymbol{\zeta}_k)\hat{\boldsymbol{e}}_k + \boldsymbol{g}_k, \quad (20)$$

where $\boldsymbol{K}(\boldsymbol{\zeta}_k)$ is an adaptive feedback gain. Thus, from (20), the mismatch error model can be rewritten as

$$\hat{\boldsymbol{e}}_{k+1} = \left[\hat{\boldsymbol{A}}(\boldsymbol{\zeta}_k) + \hat{\boldsymbol{B}}(\boldsymbol{\zeta}_k)\boldsymbol{K}(\boldsymbol{\zeta}_k)\right]\hat{\boldsymbol{e}}_k + \boldsymbol{w}_k.$$

4.4 Mismatch error adaptive controller

In order to obtain the adaptive feedback gain able to compensate the mismatch error, let $V(\hat{\boldsymbol{e}}_k) = \hat{\boldsymbol{e}}_k' \boldsymbol{P} \hat{\boldsymbol{e}}_k$ be a Lyapunov function. Moreover, let $V(\hat{\boldsymbol{e}}_k)$ be an upper bound for the LQR cost-to-go function, and consider $\boldsymbol{P} > 0$ and $V(\hat{\boldsymbol{e}}_{k+1}) - V(\hat{\boldsymbol{e}}_k) < 0$. Thus, the following optimal control problem is considered

$$V(\hat{\boldsymbol{e}}_0) \geq \min_{v[0,\infty)} \sum_{k=0}^{\infty} \hat{\boldsymbol{e}}_k' \boldsymbol{\mathcal{Q}} \hat{\boldsymbol{e}}_k + \boldsymbol{v}_k' \boldsymbol{\mathcal{R}} \boldsymbol{v}_k, \quad (21)$$

where $\boldsymbol{v}_k = \boldsymbol{K}(\boldsymbol{\zeta}_k)\hat{\boldsymbol{e}}_k$, and $\boldsymbol{\mathcal{Q}} > 0$ and $\boldsymbol{\mathcal{R}} > 0$ are, respectively, weighting matrices for the state error and control effort.

Considering (21) and the conditions for asymptotic stability, it is possible to define

$$\boldsymbol{P} > 0, \quad (22)$$

$$\hat{\boldsymbol{A}}_f' \boldsymbol{P} \hat{\boldsymbol{A}}_f + \boldsymbol{K}(\boldsymbol{\zeta}_k)' \boldsymbol{\mathcal{R}} \boldsymbol{K}(\boldsymbol{\zeta}_k) + \boldsymbol{\mathcal{Q}} - \boldsymbol{P} \leq 0 \quad (23)$$

where $\hat{\boldsymbol{A}}_f = \hat{\boldsymbol{A}}(\boldsymbol{\zeta}_k) + \hat{\boldsymbol{B}}(\boldsymbol{\zeta}_k)\boldsymbol{K}(\boldsymbol{\zeta}_k)$.

By rearranging (23), applying the Schur complement twice, and pre and post multiplying the result by a block diagonal matrix, whose diagonal is given by $\left(\boldsymbol{P}^{-1}, \boldsymbol{I}, \boldsymbol{I}, \boldsymbol{I} \right)$, the following LMI condition is obtained

$$\begin{bmatrix} \boldsymbol{S} & \boldsymbol{H}' & \boldsymbol{S}\boldsymbol{\mathcal{Q}}^{\frac{1}{2}} & \boldsymbol{Y}(\boldsymbol{\zeta})' \boldsymbol{\mathcal{R}}^{\frac{1}{2}} \\ \boldsymbol{H} & \boldsymbol{S} & 0 & 0 \\ \boldsymbol{\mathcal{Q}}^{\frac{1}{2}} \boldsymbol{S} & 0 & \boldsymbol{I} & 0 \\ \boldsymbol{\mathcal{R}}^{\frac{1}{2}} \boldsymbol{Y}(\boldsymbol{\zeta}) & 0 & 0 & \boldsymbol{I} \end{bmatrix} \geq 0, \quad (24)$$

where $\boldsymbol{S} = \boldsymbol{P}^{-1}$, $\boldsymbol{Y}(\boldsymbol{\zeta}) = \boldsymbol{K}(\boldsymbol{\zeta})\boldsymbol{P}^{-1}$, $\boldsymbol{H} = \hat{\boldsymbol{A}}(\boldsymbol{\zeta})\boldsymbol{S} + \hat{\boldsymbol{B}}(\boldsymbol{\zeta})\boldsymbol{Y}(\boldsymbol{\zeta})$.

To obtain the matrix $\boldsymbol{P}$ that shapes the Lyapunov function and fulfills the stability and performance conditions, the following optimization problem must be considered

$$\begin{aligned} \min_{\boldsymbol{S}>0,\boldsymbol{Y}(\boldsymbol{\zeta})\forall\boldsymbol{\zeta}} & \quad \text{Tr}(\boldsymbol{P}) \\ \text{s.t.} & \quad (24) \ \ \forall \boldsymbol{\zeta} \in \Delta. \end{aligned} \quad (25)$$

By knowing $\boldsymbol{P}$, the problem (23) could be reevaluated and solved explicitly for the control input $\boldsymbol{v}_k$. Thus, letting

$$\begin{aligned} f^* = \ & \hat{\boldsymbol{e}}_k^T \hat{\boldsymbol{A}}(\boldsymbol{\zeta}_k)^T \boldsymbol{P} \hat{\boldsymbol{A}}(\boldsymbol{\zeta}_k)\hat{\boldsymbol{e}}_k + \boldsymbol{v}_k^T \hat{\boldsymbol{B}}(\boldsymbol{\zeta}_k)^T \boldsymbol{P} \hat{\boldsymbol{B}}(\boldsymbol{\zeta}_k)\boldsymbol{v}_k + \hat{\boldsymbol{e}}_k^T \boldsymbol{\mathcal{Q}}\hat{\boldsymbol{e}}_k + \\ & \boldsymbol{v}_k^T \boldsymbol{\mathcal{R}}\boldsymbol{v}_k + 2\boldsymbol{v}_k^T \hat{\boldsymbol{B}}(\boldsymbol{\zeta}_k)^T \boldsymbol{P}\hat{\boldsymbol{A}}(\boldsymbol{\zeta}_k)\hat{\boldsymbol{e}}_k - \hat{\boldsymbol{e}}_k^T \boldsymbol{P}\hat{\boldsymbol{e}}_k, \end{aligned}$$

the feedback gain can be obtained by solving $\partial f^*/\partial \boldsymbol{v}_k = 0$, yielding to

$$\boldsymbol{K}(\boldsymbol{\zeta}_k) = -\left(\boldsymbol{\mathcal{R}} + \hat{\boldsymbol{B}}(\boldsymbol{\zeta}_k)^T \boldsymbol{P}\hat{\boldsymbol{B}}(\boldsymbol{\zeta}_k)\right)^{-1} \hat{\boldsymbol{B}}(\boldsymbol{\zeta}_k)^T \boldsymbol{P}\hat{\boldsymbol{A}}(\boldsymbol{\zeta}_k). \quad (26)$$

4.5 State and input constraints

To take advantage of one of the main features of predictive controllers, constraints on the amplitude of the control signal and on the state error are considered. Recalling that $\Delta \hat{\boldsymbol{x}}_k$ and $\Delta \boldsymbol{\Upsilon}_k$ are bounded by compact sets, the constraints can be written as $\Delta \hat{\boldsymbol{x}}_k \in \mathbb{E}$ and $\Delta \boldsymbol{\Upsilon}_k \in \mathbb{V}$. However, since the MPC strategy is used to obtain the pre-stabilizing control policy, the constraints must be redefined relatively to the nominal state error $\Delta \hat{\boldsymbol{x}}_k^{nom}$ and control input $\boldsymbol{g}_k$ considered in (19).

Hence, consider the reachable sets used to define regions around the nominal trajectory in order to envelop the system's states for any bounded uncertainties

$$\mathscr{R}_{k+i+1} = \left(\hat{\boldsymbol{A}}(\boldsymbol{\zeta}_k) + \hat{\boldsymbol{B}}(\boldsymbol{\zeta}_k)\boldsymbol{K}(\boldsymbol{\zeta}_k)\right) \mathscr{R}_{k+i} \oplus \mathbb{W}, \ \forall i = 0, \cdots, N_p - 1, \quad (27)$$

where N_p is the prediction horizon, $\oplus$ denotes the Minkowski sum, and $\mathscr{R}_k = \{0\}$ is the initialization condition.

Therefore, using reachable sets to reshape the bounding sets in order to have tighter constraints, it yields to

$$\begin{aligned} \bar{\mathbb{E}}_i &= \mathbb{E} \ominus \mathscr{R}_i, \quad \forall i = 1, \cdots, N_p, \\ \bar{\mathbb{V}}_i &= \mathbb{V} \ominus \boldsymbol{K}(\boldsymbol{\zeta}_k)\mathscr{R}_i, \quad \forall i = 0, \cdots, N_c - 1, \end{aligned}$$

with N_c being the control horizon and $\ominus$ denoting the Pontryagin difference.

Finally, constraints for the nominal MPC strategy can be written as

$$\Delta \boldsymbol{x}_{k+i}^{nom} \in \bar{\mathbb{E}}_i, \quad \forall i = 1, \cdots, N_p - 1, \quad (28)$$

$$\boldsymbol{g}_{k+i} \in \bar{\mathbb{V}}_i, \quad \forall i = 0, \cdots, N_c - 1. \quad (29)$$

4.6 Terminal cost and terminal constraint

Aiming to ensure closed-loop stability to the pre-stabilizing MPC policy, a terminal cost and a terminal constraint set are considered (Mayne et al., 2000).

The terminal cost able to ensure closed-loop stability for the nominal model (19) can be defined using a Lyapunov function, which is formulated as a quadratic terminal cost making use of the matrix $\boldsymbol{P}$ obtained from (25).

The terminal constraint ensuring that the last element of the predicted state sequence belongs to an invariant set is obtained by means of the one-step operator defined as

$$\tilde{Q}(\boldsymbol{\Omega}) = \left\{ \Delta \hat{\boldsymbol{x}} \in \mathbb{E} : \exists \, \boldsymbol{K}\left(\boldsymbol{\zeta}\right) \Delta \hat{\boldsymbol{x}} \in \mathbb{V}, \; \hat{\boldsymbol{A}}_f \Delta \hat{\boldsymbol{x}} + \boldsymbol{w} \in \boldsymbol{\Omega}, \; \forall \boldsymbol{w} \in \mathbb{W} \right\},$$

(30)

which must be evaluated for each vertex of Δ.

Using (30), a maximal robust control invariant set can be obtained through the iterative procedure

(1) Initialization: $\boldsymbol{\Omega}_0 = \mathbb{E} \cap \{ \omega \in \mathbb{R}^n : \boldsymbol{K}\left(\boldsymbol{\zeta}\right)\omega \in \mathbb{V}, \; \forall \boldsymbol{\zeta} \}$.
(2) Iteration: $\boldsymbol{\Omega}_{k+1} = \boldsymbol{\Omega}_k \cap \tilde{Q}(\boldsymbol{\Omega}_k)$.
(3) Terminal condition: stop when $\boldsymbol{\Omega}_{k+1} = \boldsymbol{\Omega}_k$ or $\boldsymbol{\Omega}_{k+1} = \emptyset$. Set $\boldsymbol{\Omega} = \boldsymbol{\Omega}_\infty = \boldsymbol{\Omega}_{k+1}$.

Thus, similarly to the state error, the terminal constraint set can be reshaped to define a tighter constraint for the nominal system by means of the Pontryagin difference, yielding to

$$\Delta \hat{\boldsymbol{x}}_{k+N_p}^{nom} \in \boldsymbol{\Omega} \ominus \mathscr{R}_{k+N_p}.$$

(31)

4.7 MPC strategy

Since the MPC strategy is designed to deal only with the nominal control problem, consider the cost function

$$\mathcal{J} = \sum_{i=0}^{N_p-1} \left\| \Delta \hat{\boldsymbol{x}}_{k+i}^{nom} \right\|_{\boldsymbol{Q}}^2 + \sum_{j=0}^{N_c-1} \left\| \boldsymbol{g}_{k+j} \right\|_{\boldsymbol{R}}^2 + \left\| \Delta \hat{\boldsymbol{x}}_{k+N_p}^{nom} \right\|_{\boldsymbol{P}}^2.$$

(32)

Additionally, consider, respectively, the initial state constraint and the model constraint

$$\Delta \hat{\boldsymbol{x}}_k^{nom} = \boldsymbol{0}.$$

(33)

$$\Delta \hat{\boldsymbol{x}}_{k+i+1}^{nom} = \hat{\boldsymbol{A}}(\boldsymbol{\zeta}) \Delta \hat{\boldsymbol{x}}_{k+i}^{nom} + \hat{\boldsymbol{B}}(\boldsymbol{\zeta}) \boldsymbol{g}_{k+i}, \;\; \forall i = 1, \cdots, N_p.$$

(34)

Therefore, the MPC optimization problem for the nominal system can be stated as

$$\min_{\substack{\underset{\rightarrow}{\boldsymbol{g}}, \underset{\rightarrow}{\hat{\boldsymbol{x}}}}} \mathcal{J}$$
$$\text{s.t.} \;\; (28), (29), (31), (33), (34).$$

with $\underset{\rightarrow}{\boldsymbol{g}} = [\boldsymbol{g}_k' \; \cdots \; \boldsymbol{g}_{k+N_c-1}']'$ and $\underset{\rightarrow}{\hat{\boldsymbol{x}}} = \left[(\hat{\boldsymbol{x}}_{k+1})' \; \cdots \; (\hat{\boldsymbol{x}}_{k+N_p})' \right]'$.

5. NONLINEAR INNER-LOOP CONTROLLER

This section presents the nonlinear inner-loop controller adapted from Raffo and Almeida (2018). First, the IOFL with dynamic extension technique is used to obtain a linear system through a local diffeomorphism. Hereafter, a robust discrete mixed $\mathcal{H}_2/\mathcal{H}_\infty$ controller is designed to control the resulting linear system while dealing with uncertainties coming from the decoupling procedure.

5.1 IOFL with dynamic extension

Let $\boldsymbol{h}(\boldsymbol{x}) = [z \; \phi \; \theta \; \psi]'$ be the outputs and $\boldsymbol{u} = [f_R \; f_L \; \tau_{\alpha_R} \; \tau_{\alpha_L}]'$ be the inputs of the system (7). Therefore, considering (10), a system affine in the control inputs can be written as

$$\dot{\boldsymbol{x}} = \boldsymbol{f}(\boldsymbol{x}) + \boldsymbol{g}_{\boldsymbol{u}}(\boldsymbol{x})\boldsymbol{u} + \boldsymbol{g}_{\boldsymbol{d}}(\boldsymbol{x})\boldsymbol{\delta},$$
$$\boldsymbol{y} = \boldsymbol{h}(\boldsymbol{x}).$$

(35)

The system relative degree is given by the sum of all outputs' relative degree $r = \sum r_i$, where $r_i =$

$\inf \left\{ k : \exists j, \mathcal{L}_{\boldsymbol{g}_j} \mathcal{L}_{\boldsymbol{f}}^{k-1} h_i(\boldsymbol{x}) \neq 0 \right\}$, with $\boldsymbol{g}_j$ being the j-th column of $\boldsymbol{g}_{\boldsymbol{u}}(\boldsymbol{x})$, $h_i(\boldsymbol{x})$ the i-th output, and $\mathcal{L}_{\boldsymbol{f}} h$ the Lie Derivative of $\boldsymbol{h}$ in the direction of $\boldsymbol{f}$.

To obtain a system with a set of inputs/outputs fully feedback linearizable, its relative degree should be equal to the number of state variables. However, the system (35) is not fully feedback linearizable since its relative degree is $r = 8$ with $\boldsymbol{x} \in \mathbb{R}^{12}$. To overcome this issue, the dynamic extension technique is used by augmenting the state vector to $\bar{\boldsymbol{x}} = \begin{bmatrix} \boldsymbol{q}' & \dot{\boldsymbol{q}}' & f_R & \dot{f}_R & f_L & \dot{f}_L \end{bmatrix}'$ and redefining the input vector as $\bar{\boldsymbol{u}} = \begin{bmatrix} \ddot{f}_R & \ddot{f}_L & \tau_{\alpha_R} & \tau_{\alpha_L} \end{bmatrix}'$, which leads to

$$\dot{\bar{\boldsymbol{x}}} = \bar{\boldsymbol{f}}(\bar{\boldsymbol{x}}) + \sum_{i=1}^{4} \bar{\boldsymbol{g}}_i(\bar{\boldsymbol{x}})\bar{\boldsymbol{u}}_i + \bar{\boldsymbol{g}}_{\boldsymbol{d}}(\bar{\boldsymbol{x}})\boldsymbol{\delta},$$
$$\boldsymbol{y} = \boldsymbol{h}(\boldsymbol{x}),$$

(36)

where $\bar{\boldsymbol{f}}(\bar{\boldsymbol{x}}) = \begin{bmatrix} \dot{\boldsymbol{q}}' & \ddot{\boldsymbol{q}}' & \dot{f}_R & 0 & \dot{f}_L & 0 \end{bmatrix}'$, $\ddot{\boldsymbol{q}} = \boldsymbol{M}^{-1}\left(-\left[\boldsymbol{C} + \boldsymbol{\mu} \right] \dot{\boldsymbol{q}} - \boldsymbol{G} + \boldsymbol{\delta} \right) + \boldsymbol{B}_1 f_R + \boldsymbol{B}_2 f_L$, $\bar{\boldsymbol{u}}_i$ is the i-th input of $\bar{\boldsymbol{u}}$, $\boldsymbol{B}_i$ is the i-th column of $\boldsymbol{B}$, and $\bar{\boldsymbol{g}}_i(\bar{\boldsymbol{x}})$ is given by

$$\bar{\boldsymbol{g}}_1 = \begin{bmatrix} \boldsymbol{0}_{13\times1} \\ 1 \\ \boldsymbol{0}_{2\times1} \end{bmatrix}, \bar{\boldsymbol{g}}_2 = \begin{bmatrix} \boldsymbol{0}_{15\times1} \\ 1 \end{bmatrix}, \bar{\boldsymbol{g}}_3 = \begin{bmatrix} \boldsymbol{0}_{6\times1} \\ \boldsymbol{B}_3 \\ \boldsymbol{0}_{4\times1} \end{bmatrix}, \bar{\boldsymbol{g}}_4 = \begin{bmatrix} \boldsymbol{0}_{6\times1} \\ \boldsymbol{B}_4 \\ \boldsymbol{0}_{4\times1} \end{bmatrix}.$$

The relative degree of the augmented system (36) is $r = 16$ with $\bar{\boldsymbol{x}} \in \mathbb{R}^{16}$, which is now fully feedback linearizable.

In order to obtain the transformed linearized system, the input transformation is considered

$$\bar{\boldsymbol{u}} = \boldsymbol{\Delta}^{-1}(\boldsymbol{v} - \boldsymbol{b}),$$

with $\boldsymbol{v} = \begin{bmatrix} v_z & v_\phi & v_\theta & v_\psi \end{bmatrix}'$ being additional control inputs. Considering $\bar{\boldsymbol{x}}$ and $\bar{\boldsymbol{u}}$, it is possible to define

$$\boldsymbol{\Delta}(\bar{\boldsymbol{x}}) \in \mathbb{R}^{4\times4} \;:\; \boldsymbol{\Delta}_{ij}(\bar{\boldsymbol{x}}) = \mathcal{L}_{\bar{\boldsymbol{g}}_j} \mathcal{L}_{\bar{\boldsymbol{f}}}^3 h_i(\bar{\boldsymbol{x}}),$$
$$\boldsymbol{b}(\bar{\boldsymbol{x}}) \in \mathbb{R}^{4\times1} \;:\; \boldsymbol{b}_i(\bar{\boldsymbol{x}}) = \mathcal{L}_{\bar{\boldsymbol{f}}}^4 h_i(\bar{\boldsymbol{x}}),$$

where $\boldsymbol{\Delta}_{ij}(\bar{\boldsymbol{x}})$ is the (i,j)-th entry of the matrix $\boldsymbol{\Delta}(\bar{\boldsymbol{x}})$ and $\boldsymbol{b}_i(\bar{\boldsymbol{x}})$ is the i-th row of $\boldsymbol{b}(\bar{\boldsymbol{x}})$. Therefore, the system's outputs are given by the linear relation $\boldsymbol{y}^{(r)} = \ddddot{\boldsymbol{h}}(\bar{\boldsymbol{x}}) = \boldsymbol{v} + \boldsymbol{\pi}(\boldsymbol{\delta})$, with $\boldsymbol{\pi}(\boldsymbol{\delta})$ being a term containing unmodeled dynamics and unknown external disturbances.

Thereafter, a PID-like controller with feed-forward term is used to regulate the outputs z, ϕ, θ, and ψ. The additional linear control laws can be designed as

$$v_i = \ddddot{i}^{tr} + K_{ddd_i}\ddddot{e}_i + K_{dd_i}\dddot{e}_i + K_{d_i}\dot{e}_i + K_{p_i}e_i + K_{i_i}\int e_i dt,$$

where $e_i = i - i^{tr}$ with $i \in \{z, \phi, \theta, \psi\}$ and $(\cdot)^{tr}$ denoting the desired trajectory.

Defining the vector $\tilde{\boldsymbol{e}} = \begin{bmatrix} \int \boldsymbol{e} dt & \boldsymbol{e} & \dot{\boldsymbol{e}} & \ddot{\boldsymbol{e}} & \dddot{\boldsymbol{e}} \end{bmatrix}'$ with $\boldsymbol{e} = [e_z \; e_\phi \; e_\theta \; e_\psi]'$, and $\boldsymbol{K} = \mathbf{blkdiag}\left(K_i, K_p, K_d, K_{dd}, K_{ddd}\right)$, the linearized dynamics can be written as

$$\dot{\tilde{\boldsymbol{e}}} = \boldsymbol{A}\tilde{\boldsymbol{e}} + \boldsymbol{B}_{\boldsymbol{u}}\tilde{\boldsymbol{u}} + \boldsymbol{B}_{\boldsymbol{\pi}}\boldsymbol{\pi},$$
$$\tilde{\boldsymbol{u}} = \boldsymbol{K}\tilde{\boldsymbol{e}}.$$

(37)

5.2 Discrete mixed $\mathcal{H}_2/\mathcal{H}_\infty$ control

To design a discrete mixed $\mathcal{H}_2/\mathcal{H}_\infty$ control to compute the feedback gain $\boldsymbol{K}$, the model (37) must be discretized with a sampling time T_{si}, yielding to

$$\tilde{\boldsymbol{e}}_{k+1} = \boldsymbol{A}\tilde{\boldsymbol{e}}_k + \boldsymbol{B}_{\boldsymbol{u}}\tilde{\boldsymbol{u}}_k + \boldsymbol{B}_{\boldsymbol{\pi}}\boldsymbol{\pi}_k,$$
$$\tilde{\boldsymbol{u}}_k = \boldsymbol{K}\tilde{\boldsymbol{e}}_k.$$

(38)

Considering the $\mathcal{H}_2$ norm and the $\mathcal{H}_\infty$ norm of the system (38) as proposed by Rego and Raffo (2016), the feedback gain $\boldsymbol{K}$ that minimizes an upper-bound for the $\mathcal{H}_2$ norm while guaranteeing a prescribed upper-bound $\sqrt{\bar{\varrho}} > \sqrt{\varrho}$ for the $\mathcal{H}_\infty$ norm can be obtained by means of LMIs

$$\begin{bmatrix} N & HX + D_u Y \\ * & X + X^T - P \end{bmatrix} > 0, \qquad (39)$$

$$\begin{bmatrix} P & AX + B_u Y & B_\pi & 0 \\ * & X + X^T - P & 0 & X^T H^T + Y^T D_u^T \\ * & * & I & D_\pi^T \\ * & * & * & \tilde{\varrho} I \end{bmatrix} > 0, \qquad (40)$$

where $*$ denotes the elements that are deduced by symmetry, $K = -YX^{-1}$, and H, D_u, and D_π are weighting matrices.

Furthermore, the system's time response can be improved by means of pole placement constraints using LMIs regions to restrict the complex plane as proposed by Rego and Raffo (2016). Therefore, the LMIs conditions are given by

$$TA^T + AT + Y^T B_u^T + B_u Y - 2\varepsilon T > 0, \qquad (41)$$

$$\begin{bmatrix} -\varpi T & AT + B_u Y \\ * & -\varpi T \end{bmatrix} < 0, \qquad (42)$$

where $\{\varepsilon, \varpi\} \in \mathbb{R}^+$. The constraints (41) and (42) can be merged into the mixed $\mathcal{H}_2/\mathcal{H}_\infty$ control problem by making $X = X^T = T > 0$.

Finally, the feedback gain K to control the system (38) can be obtained solving the optimization problem

$$\min_{P, X, Y, N} \quad \text{Tr}(N)$$
$$\text{s.t.} \quad (39) - (42)$$

with $\text{Tr}(\cdot)$ denoting the trace operator.

6. NUMERICAL SIMULATIONS RESULTS

This section presents the simulation results obtained with the proposed cascade control strategy performing trajectory tracking of a Tilt-rotor UAV carrying a suspended load with dynamics described by the nonlinear model (1).

Considering the limits for the state error and for the intermediary control input, $\Delta x = [-1, 1]$, $\Delta y = [-1, 1]$, $\Delta \gamma_1 = [-0.5, 0.5]$, $\Delta \gamma_2 = [-0.5, 0.5]$, $\Upsilon_1 = [-13, 13]$, and $\Upsilon_2 = [-15, 15]$, the bounding sets are given by

$$\mathbb{E} = \{\Delta x, \Delta y \in \pm 1 \text{ [m]}, \Delta \gamma_1, \Delta \gamma_2 \in \pm 0.5 \text{ [rad]}\},$$
$$\mathbb{V} = \{\Upsilon_1 \in \pm 13, \Upsilon_2 \in \pm 15\},$$
$$\mathbb{W} = \{w_x, w_y \in \pm 0.1 \text{ [m]}, w_{\gamma_1}, w_{\gamma_1} \in \pm 0.01 \text{ [rad]}\},$$

with $\mathbb{V}$ being obtained through (12) at the values γ_1^{eq}, γ_2^{eq}, $\phi = [-0.5, 0.5]$, $\theta = [-0.5, 0.5]$, $f_R = [0, 15]$, and $f_L = [0, 15]$; and $\mathbb{W}$ being chosen by try-and-error.

Using the Bryson's rule (Johnson and Grimble, 1987) as initial tune, and followed by a fine adjustment, the weighting matrices $\mathcal{Q}$ and $\mathcal{R}$ are chosen as

$$\mathcal{Q} = \text{diag}\left(\frac{1}{2^2}, \frac{1}{2^2}, \frac{5}{(\pi/2)^2}, \frac{5}{(\pi/2)^2}, \frac{1}{2^2}, \frac{1}{2^2}, \frac{1}{(3\pi)^2}, \frac{1}{(3\pi)^2}, 10, 10\right),$$

$$\mathcal{R} = \text{diag}\left(\frac{1}{(13 - \Upsilon_1^{eq})^2}, \frac{1}{(15 - \Upsilon_2^{eq})^2}\right).$$

The prediction and control horizons, chosen considering a trade-off between good performance and computational cost, are $N_p = 5$ and $N_c = 2$. The maximum absolute accelerations are 1 [m/s²], which gives the polytope $\Delta = \{\pm 1, \pm 1\} \in \mathbb{R}^2$. Further, the sampling times for discretization purposes are $T_{si} = 12$ and $T_{so} = 120$ given in milliseconds.

Moreover, the system physical parameters are given by: $d_{\mathcal{C}_1}^{\mathcal{B}} = [-0.433\ 0.060\ -4.559]' \cdot 10^{-2}$, $d_{\mathcal{C}_2}^{\mathcal{B}} = [0.002\ -27.761\ 5.493]' \cdot 10^{-2}$, and $d_{\mathcal{C}_3}^{\mathcal{B}} = [0.077\ 27.761\ 5.493]' \cdot 10^{-2}$ given in [m]; $m_1 = 1.70249$, $m_2 = m_3 = 0.13973$, and $m_4 = 0.090$ given in [Kg];

$g_z = 9.81$ [m/s²]; $k_d = 0.01789$ [m]; $\beta = 5°$; $l = 1$ [m]; $\mu_\gamma = 0.005$ [N·m/(rad/s)]; and the inertia moment of the *i-th* body in relation to the axes j and k, I_i^{jk}, given in 10^{-6}[Kg.m²] by $I_1^{xx} = 3697.66749$, $I_1^{yy} = 840.10403$, $I_1^{zz} = 3865.05354$, $I_1^{xy} = 0.36342$, $I_1^{xz} = -9.51029$, $I_1^{yz} = 0.61804$, $I_2^{xx} = I_3^{xx} = 441.68245$, $I_2^{yy} = I_3^{yy} = 441.67985$, $I_2^{zz} = I_3^{zz} = 0.64418$, $I_2^{xy} = I_3^{xy} = 0$, $I_2^{xz} = I_3^{xz} = 0$, $I_2^{yz} = -I_3^{yz} = -1.07006$, $I_4^{xx} = I_4^{yy} = I_4^{zz} = 2.645$.

The presented simulations were carried out using the MATLAB/Simulink® environment and the toolboxes YALMIP and MPT (Löfberg, 2004; Herceg et al., 2013).

Fig. 2 shows the results of the Tilt-rotor UAV carrying a suspended load while performing a square-like trajectory when affected by the disturbances shown in Fig. 3. The tube-based MPC controls the system's planar motion and provides the load stabilization. The nonlinear inner-loop IOFL controller deals with the altitude and the yaw regulation, while stabilizes the remaining degrees of freedom of the system. Moreover, Fig. 2 shows a small load swing due to the trajectory changes of direction that is being reduced throughout the execution by the tube-based MPC.
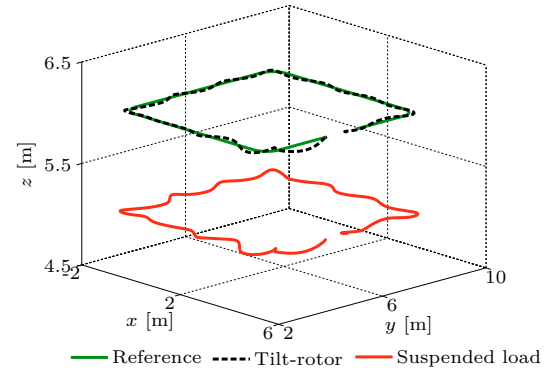
Fig. 2. Trajectory tracking using the proposed controllers.
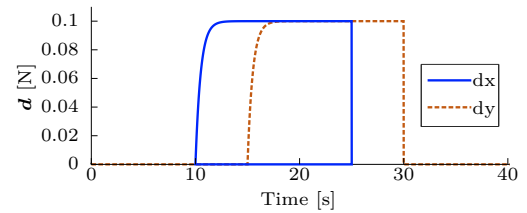
Fig. 3. Profile of the disturbance forces.

Fig. 4 presents the time evolution of the regulated variables x, y, z, and ψ. The proposed tube-based MPC successfully performs trajectory tracking for the states x and y, as well as, the nonlinear controller for z and ψ. As seen in Fig. 4, the yaw movements are considered in order to perform trajectory tracking always head-on to the trajectory, which is possible due to the nonlinear IOFL controller.

Furthermore, Fig. 5 shows that the remaining system's degrees of freedom are kept stable during the trajectory execution, meaning that the cascade structure composed by the tube-based MPC and the nonlinear IOFL controller was able to ensure closed-loop stability for the Tilt-rotor UAV during the considered simulation scenario. Some oscillatory behaviors, despite being small, can be seen in Fig. 5. They are mainly due to the load swing and are being attenuated along the trajectory by the controllers in order to avoid the system to destabilize. Also, Fig. 6 shows that the

input signals computed by the inner-loop controller did not saturate the vehicle's actuators. Moreover, it is possible to notice that some peaks appear in the torque input signals, which is explained by the required direction change in the corners of the square-like trajectory.
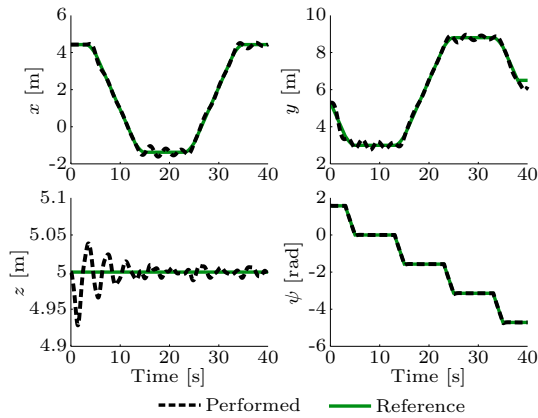
Fig. 4. Time evolution of the regulated variables.
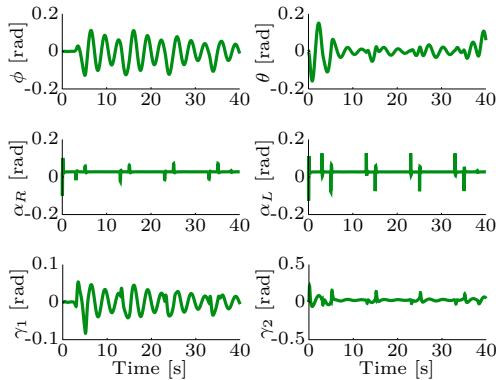
Fig. 5. Time evolution of the remaining degrees of freedom.
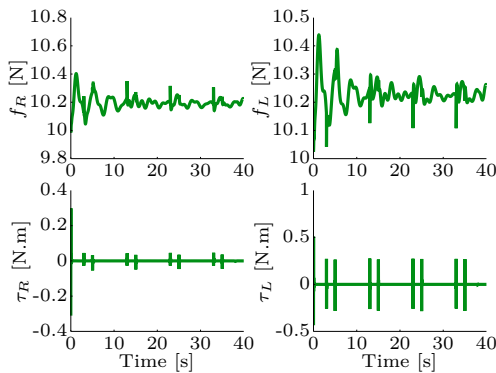
Fig. 6. Inputs applied to the Tilt-rotor UAV.

7. CONCLUSION

This paper proposed a hierarchical control strategy to solve the trajectory tracking problem of a Tilt-rotor UAV with suspended load operating in helicopter flight-mode. The system's equations of motion were described and decoupled in order to control separately the dynamics related to the planar position and the load stabilization from the remaining dynamics. For the inner-loop, a nonlinear controller using the IOFL with dynamic extension technique and a robust discrete mixed $\mathcal{H}_2/\mathcal{H}_\infty$ was developed. As for the outer-loop, a tube-based MPC strategy was designed aiming to add features into the problem as constraints satisfaction and prediction of future states without losing robustness. Further, simulation results were presented corroborating the control strategy good performance. In future works, experimental results will be obtained and ways to reduce the tube-based MPC computational cost will be addressed aiming to perform whole body control, extending the MPC features for every system's degrees of freedom. Besides, identification techniques aiming to represent the system as an LPV model will be considered to design the proposed tube-based MPC strategy with an enlarged domain of attraction, which could allow yaw movements regulation despite being a linearized control strategy.

REFERENCES

Almeida, M. and Raffo, G. (2015). Nonlinear control of a tiltrotor UAV for load transportation. In *Proc. of SYROCO*, 234–239.

Amiri, N., Ramirez-Serrano, A., and Davies, R. (2013). Integral backstepping control of an unconventional dual-fan unmanned aerial vehicle. *Journal of Intelligent & Robotic Systems*, 69(1), 147–159.

Bernard, M. and Kondak, K. (2009). Generic slung load transportation system using small size helicopters. In *Proc. of ICRA*, 3258–3264.

Dai, S., Lee, T., and Bernstein, D. (2014). Adaptive control of a quadrotor uav transporting a cable-suspended load with unknown mass. In *Proc. of CDC*, 6155–6160.

Gonzalez, R., Fiacchini, M., Alamo, T., Guzman, J., and Rodriguez, F. (2011). Online robust tube-based mpc for time-varying systems: a practical approach. *International Journal of Control*, 84(6), 1157 – 1170.

Herceg, M., Kvasnica, M., Jones, C., and Morari, M. (2013). Multi-parametric toolbox 3.0. In *Proc. of ECC*, 502–510.

Johnson, M. and Grimble, M. (1987). Recent trends in linear optimal quadratic multivariable control system design. *IEE Proc. Control Theory Appl.*, 134(1), 53–71.

Langson, W., Chryssochoos, I., Raković, S., and Mayne, D. (2004). Robust model predictive control using tubes. *Automatica*, 40(1), 125–133.

Löfberg, J. (2004). Yalmip: A toolbox for modeling and optimization in matlab. In *Proc. of CACSD*.

Mayne, D., Rawlings, J., Rao, C., and Scokaert, P. (2000). Constrained model predictive control: Stability and optimality. *Automatica*, 36(6), 789–814.

Papachristos, C., Alexis, K., and Tzes, A. (2013). Model predictive hovering-translation control of an unmanned tri-tiltrotor. In *Proc. of ICRA*, 5425–5432.

Raffo, G. and Almeida, M. (2018). A load transportation nonlinear control strategy using a tilt-rotor uav. *Journal of Advanced Transportation*, 2018, 1–20.

Rego, B. and Raffo, G. (2016). Suspended load path tracking control based on zonotopic state estimation using a tilt-rotor UAV. In *Proc. of ITS*, 1445–1451.

Sreenath, K., Michael, N., and Kumar, V. (2013). Trajectory generation and control of a quadrotor with a cable-suspended load - a differentially-flat hybrid system. In *Proc. of ICRA*, 4873–4880.

Yanguo, S. and Huanjin, W. (2009). Design of flight control system for a small unmanned tilt rotor aircraft. *Chinese Journal of Aeronautics*, 22(3), 250–256.